Comparative Analysis of a Numerical Model with Direct N-body and Monte Carlo Simulations of Binary Black Hole Formation in Stellar Clusters

Roman A. Mikhaylenko*
Dept. Física Quàntica i Astrofísica, Universitat de Barcelona
(Dated: June 22, 2020)

Black hole (BH) binary mergers are a natural occurrence in the evolution of stellar clusters. This work presents some of the current simulational models of various computational requirements and compares their results, with special focus on BH merger production. The main objective is to identify systematic differences in output of the fastest model considered, clusterBHBdynamics, with the other models, and identify physical processes in the evolution of globular clusters (GCs) which could account for these differences. This study finds discrepancies in the number of mergers in lower-mass GCs, with clusterBHBdynamics producing 78.0 ± 39.1 times less mergers in the least massive clusters considered. To account for this difference, Kozai-Lidov oscillations in hierarchical triples are identified as a mechanism which could be implemented to yield a higher number of mergers in low-mass clusters. Further second order corrections are discussed for completeness and future exploration of the model.

1. INTRODUCTION

On September 14, 2015 the Laser Interferometer Gravitational-Wave Observatory (LIGO) observed a transient gravitational wave (GW) signal for the first time (Aarseth 2012; Abbott 2017a). It matched the waveform predicted by general relativity (GR) for the inspiral and merger of a pair of black holes with a significance greater than 5.1σ. Since then, over 40 candidate merger events have been identified by LIGO and the European Gravitational Observatory (EGO), with the planned KAGRA and INDIGO detectors expected to provide further insight during this decade. (Liu et al. 2020; Kuroda and LCGT Collaboration 2010; Mann 2020).

These discoveries are stimulating the field of compact object binaries and generating great interest in understanding how these systems form. The mechanisms put forward consider the environments the binaries evolve in, such as the fields of galaxies, hierarchical multiple field stars, young stellar clusters and globular clusters.

This work considers the latter scenario, namely binary BH formation in globular clusters of all masses. Higher mass globular clusters ($>1.0\text{x}10^5 M_\odot$) naturally draw more attention due to higher BH formation rates, and have been simulated numerically in Banerjee 2017; Banerjee 2018a; Banerjee 2018b; Banerjee 2020 and Rodriguez et al. 2018. However, the cluster initial mass function of GCs is a power-law with index -2 (Portegies Zwart, McMillan, and Gieles 2010; Jordán et al. 2007), and smaller mass clusters ($<1.0\text{x}10^4 M_\odot$) are more abundant, thus could contribute significantly to the total BBH population.

The dense core of a stellar cluster facilitates the formation of BH binaries through three body processes, which subsequently harden and coalesce via binary-single interactions. These binaries are expected to comprise a formidable fraction of all binary BH mergers detected so far (Kumamoto, Fujii, and Tanikawa 2020; Fragione and Kocsis 2018). Currently, the most accurate and detailed cluster evolution simulations are based on star-by-star N-body or Monte Carlo approaches (Banerjee 2020; Rodriguez et al. 2018; Mirek Giersz et al. 2013) and allow for simultaneous development of stellar and binary evolution, galactic tides, primordial binaries, relativistic corrections during close interactions and other parameters. For this reason, they are able to thoroughly simulate

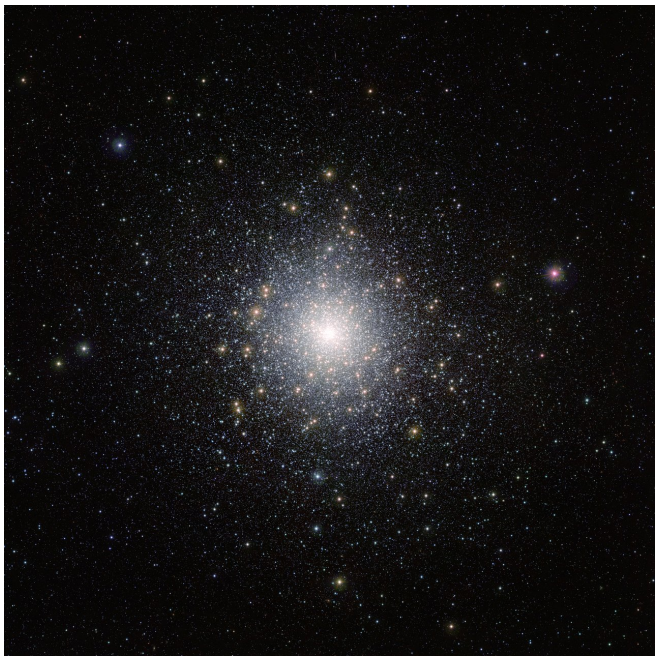

Figure 1: 47 Tucanae (NGC 104), one of the most massive globular clusters ($\sim 1.0\text{x}10^6 M_\odot$, Lane et al. 2010) and therefore potentially an important contributor of BBH. Observed with the ESO/VISTA telescope. Credit: ESO/M.-R. Cioni/VISTA Magellanic Cloud survey.

*Electronic address: rmikhami27@alumnes.ub.edu

stellar dynamical relaxation of a cluster self consistently. Unfortunately, such elaborate models come at an expensive computational cost, and published simulations are generally restricted to a limited set of initial cluster conditions (Banerjee 2020; Rodriguez et al. 2018; Fragione and Kocsis 2018).

With this limitation in mind, Antonini and Gieles 2020 presented a fast computational method for the evolution of a star cluster with BHs, including a prescription for the dynamical evolution of BH binaries. The Banerjee 2017-Banerjee 2020 series and Gupta et al. 2020 showed that low-mass clusters are efficient contributors to BBH mergers, more than what is expected from extrapolating the mass dependence from massive cluster models. This is the main motivation for this study - to compare Antonini and Gieles 2020's model against the published results from N-body and Monte Carlo simulations, with emphasis on low-mass clusters in the context of BH mergers.

The paper is organised as follows. Sections 2 and 3 introduce the coevolution of stellar clusters and their BH and BBH populations, and how they can be simulated. Section 4 presents the state-of-the-art direct N-body, Monte Carlo and numerical models used to simulate dynamical interactions, eccentricities and BBH merger rates. Section 5 discusses the methodology implemented in comparing clusterBHBdynamics against other models using published literature, with special focus on BH merger-related outputs at low masses. Finally, in section 6, the findings of the comparison are explored in the context of physical mechanisms that could be responsible for responsible for any differences, and potential adjustments to Antonini and Gieles 2020's model are suggested.

2. GLOBULAR CLUSTER EVOLUTION MECHANICS

Stellar clusters can be classified according to their mass and age. Open clusters are young (10-100 Myr), low mass (100-1000$M_\odot$) clusters and are typically found in the disk. Young massive clusters are young (few Myrs), massive ($1.0x10^5 M_\odot$) and found in starburst galaxies. Globular clusters are old (10-12 Gyr), massive ($1.0x10^5 M_\odot$) and are located in the halo. Globular clusters are abundant structures, with over 150 found in the Milky Way so far (Ashman and Zepf 1992; Antonini, Barausse, and Silk 2015) and are the focus of this paper.

Globular clusters are spherical collections of stars that orbit galaxies. They are tightly bound by gravity, which gives them their spherical shapes and relatively high stellar densities toward their centres ($\sim 1.0x10^6 M_\odot/pc^{-3}$). Due to their dense cores, they are considered collisional systems and thus give rise to some exotic classes of objects, such as blue stragglers, millisecond pulsars, and binary black holes (BBH) (Leonard 1989). The mass of black holes is highly dependent on the mass and metallicity of the parent stars. It is generally accepted that higher metallicity in stars leads to higher mass loss through stellar winds, resulting in lower mass BHs. Therefore, because lower mass BBHs are less efficient in providing energy to the cluster, metal-rich clusters form BBH at a higher rate (Antonini and Gieles 2020). Metallicity evolves on cosmological timescales (GCs are old and formed when the universe formed, and have low Z) and is strongly correlated with BH production. For example, the star formation rate (SFR) is lower now compared to the early universe, however since metal-rich stars make more BHs, the rate of BBH formation is higher today. Thus it is of great interest to consider the numerous (fig. 2), recently-formed, small mass clusters, where high Z can outweigh the lack of mass. These smaller mass clusters tend to be found at smaller distances from the galactic centres and may operate additional evolutionary mechanisms, compared to their more massive companions (Gupta et al. 2020).

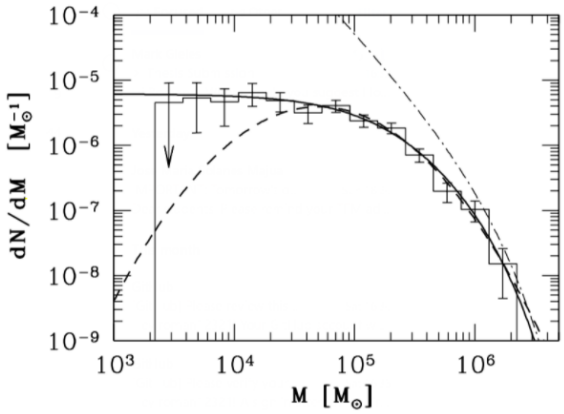

Figure 2: The solid line shows Jordán et al. 2007's GC mass distribution, dN/dM, for the Milky Way, where M is the mass of the GC and N is the number in the corresponding M bin. Corresponding uncertainties and model fits are derived from the GC luminosity function. Low-mass GCs ($\leq 1.0x10^4 M_\odot$) significantly outnumber the massive ones ($\geq 1.0x10^5 M_\odot$), suggesting that a BH merger production of even an order of magnitude smaller in low-mass clusters can contribute greatly to the overall population.

3. BBH FORMATION AND INSPIRAL MECHANICS

To appreciate the complexity of the models under consideration in this paper, we explore some key mechanisms being simulated. The first stage in the production of a GW inspiral is a compact object binary. Since GCs are collisional systems, 3 body encounters make copious amounts of BH binaries, only a small fraction of which do not disrupt instantaneously. This is attributed to the 'hardness' of the binary and is a function of the kinetic energy of the surrounding bodies. Soft binaries have energy $E_{bin} > K_3$ where E_{bin} is the energy of the

binary and K_3 is the kinetic energy of the fly-by. During these interactions, soft binaries gain energy from the third body, increasing their orbital separation and eventually becoming unbound (fig. 3). Hard binaries have $E_{bin} < K_3$ and exhibit the opposite behaviour, transferring energy to the third body, decreasing their orbital separation and spiralling into more circular, tightly-bound orbits. It is estimated that around 20% of a binary's energy is lost or gained in every such interaction, implying a tightening or loosening of 20%, as seen by the generally increasing jumps in orbital separation with evolution in time in fig. 3. Statistically, this is a positive feedback mechanism for soft binaries: increasing the orbital radius with each interaction increases the probability of another interaction. On the contrary, hard binaries would experience the opposite in a uniform distribution of bodies. However, density decreases with radius in globular clusters and in-cluster BBH gravitationally sink into, and are almost always located in the centre of a cluster, boosting the rate of three-body interactions to statistical significance.

As a binary hardens and loses energy, its orbital eccentricity reduces until near-circular rotation ensues. Then, equation energy loss via the emission of GW drives the binary to a merger in the absence of further collisions.

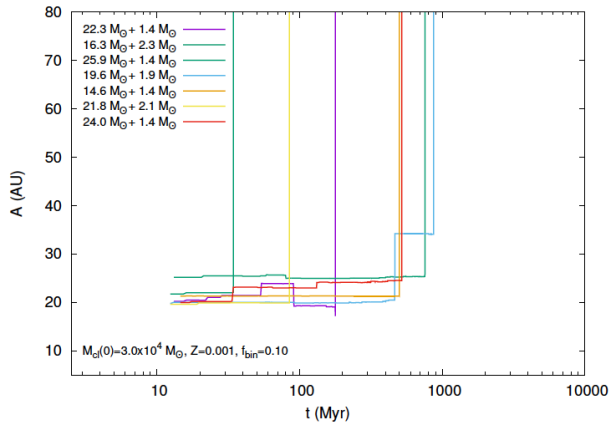

Figure 3: Examples of time evolution of the semi-major-axes, A, of the NS-BH binaries from Banerjee 2018a, as a proxy for BH-BH pairs. Each line follows a particular soft NS-BH binary. In general, the increments in A increase with A, as a consequence of a ∼20% of energy and momentum transfer in every interaction. Their in-cluster lifetimes, vary from 100 Myr to Gyrs, when the pairs are destroyed, often through exchange interactions.

This 20% transfer of energy (and thus momentum) per collision sets a limit on the time a hard binary spends inside a cluster. Newton's III law implies that by conservation of momentum, a binary eventually attains a common velocity v_{bin} that is higher than the escape velocity v_{esc} of the cluster. A simple geometric progression calculation shows that $v_{bin} > v_{esc}$ after the binary has ejected about 7 single BHs, for typical v_{esc} (a factor of around 5-10 times greater than the velocity dispersion of the cluster)(Antonini and Gieles 2020). Furthermore, SN kicks contribute to the displacement of BH from the core.

Therefore, ejection is the fate of most BH binaries. The loss of mass from the cluster by ejection causes the cluster to expand and the density of the core increases, providing some indirect heat to the cluster. After some time, a new binary is needed and the core contracts again to form another 3-body binary. On timescales of Gyr, while the cluster ejects BBHs, the radius increases and stars are lost over the tidal boundary, i.e. the cluster is dissolved and becomes less efficient in producing tightly bound BBHs. The dissolution is typically measured with respect to time as a proxy, however the real drivers are SN kicks and dynamical collisions.

A sidenote on the eccentricities of binaries: while eccentricities are not discussed at length in this paper, they play a crucial role in the formation of BH mergers. High eccentricity can reduce the semi-major axis sufficiently to lead to a merger by gravitational capture, or significant GW emission at the point of closest approach, removing energy from the system and eventually causing an inspiral.

These key mechanisms of BH binaries and initial conditions of stellar clusters are considered and incorporated in state-of-the-art models.

3.1. Modelling Cluster Evolution

Like with many new concepts in physics, the assumption of a Boltzmann distribution was made as a first iteration to model stellar clusters. Fig. 4 shows that to a good approximation, the Plummer 1911 potential along with the collisionless Boltzmann equation have been used to replicate the gravitational potential of star clusters (Merafina, Piscicchia, and Donnari 2018,Lane et al. 2010). Later on, in order to adjust for the gravothermal catastrophe, the Fokker-Planck equation was introduced by Spitzer and Harm 1958, combining the equilibria established by energy exchange in collisions among stars, and by the removal of stars with the highest kinetic energy by the host galaxy's tidal forces. This yielded a robust model for application in evolutionary simulations(Antonov 1962).

More recently, Gieles and Zocchi 2015 presented a family of self-consistent, spherical, lowered isothermal models. They are particularly suited to describe the phase-space density of stars in tidally limited star clusters in all stages of their life-cycle, and thus are excellent for comparison with data of resolved GCs.

One interesting result of thermodynamics of GCs is that the temperature gradient in a (virialised) stellar system increases as a result of two-body relaxation. In other words, as a self-gravitating system cools, it actually heats up (in the center). This heating is significant for the formation of BBH, since they reside in the centres of GCs (Hénon 1975).

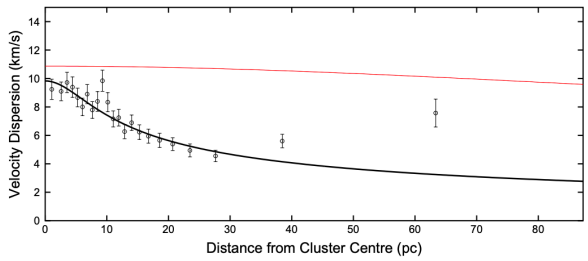

Figure 4: AAOmega Observations of 47 Tucanae. Binned velocity dispersion as a function of radius with the radial velocity profiles of the two stellar populations from the best fit double Plummer model. The Plummer profile that dominates at small radii is shown as the thick black curve, while the thin curve shows the Plummer profile for the stellar population that dominates at large radii. This model still serves as an approximation in many models today (Lane et al. 2010).

4. NBODY7 VS CLUSTERBHBDYNAMICS

This study is mainly concerned with two stellar cluster evolution models. The first is clusterBH[1] & BHBdynamics[2], presented in Antonini and Gieles 2020 and used in combination for complete performance. They are therefore referred to as clusterBHBdynamics. The second model is NBODY7, a powerful direct N-body code, the latest version of which can be found in Banerjee 2020.

Published NBODY7 runs were performed on server computers containing NVIDIA, Fermi-, Kepler-, or Turing-series GPUs and 4- or 16-thread CPUs, and took about a year to complete (Banerjee 2020). In contrast, any run on clusterBHBdynamics can be processed in seconds on a commercial laptop.

4.1. NBODY7

The NBODY7 code is extremely versatile and facilitates the treatment of continuous formation of multiple systems that dynamically affect their own evolution, especially of those involving massive objects like BHs ((Abbott 2017b; Nitadori and Aarseth 2012)). The stellar parameters or each star (including any tidal effect if it is a member of a binary or a multiple) are updated simultaneously with its trajectory integration. That way the effects of stellar evolutionary mass loss, via winds and supernovae, are naturally incorporated in a calculation. An important aspect of NBODY7 is its general relativistic (GR) treatment, when an NS or/and a BH is a member of binary or a multiplet. Complete information on the implementation of GW merger kicks due to BH spins, SN kicks and other mechanisms discussed in sections 2 & 3 can be found in Banerjee 2020.

In the data used for this study, the computed models are initially Plummer clusters for masses $7.0\text{x}10^3\text{M}_\odot \leq M_{cl} \leq 1.0\text{x}10^5\text{M}_\odot$, as is typical for Galactic and Local Group star clusters (Banerjee and Kroupa 2017; Portegies Zwart, McMillan, and Gieles 2010). As mentioned previously, the computational cost for these calculations is large, and therefore the range of initial conditions simulated in published literature is relatively limited. For example, clusters with $r_{h0} = 2$ pc have been tested more than 1pc and masses were capped at $1.0\text{x}10^5\text{M}_\odot$ to optimize processing time. All clusters were evolved for 11 Gyr or unless they dissolved completely earlier.

A multitude of parameters can be extracted from the evolved NBODY7 code, one example of which is given in fig. 5, showing how the BH depletion with time, discussed in section 3, is exacerbated by increasing the metallicity of the cluster.

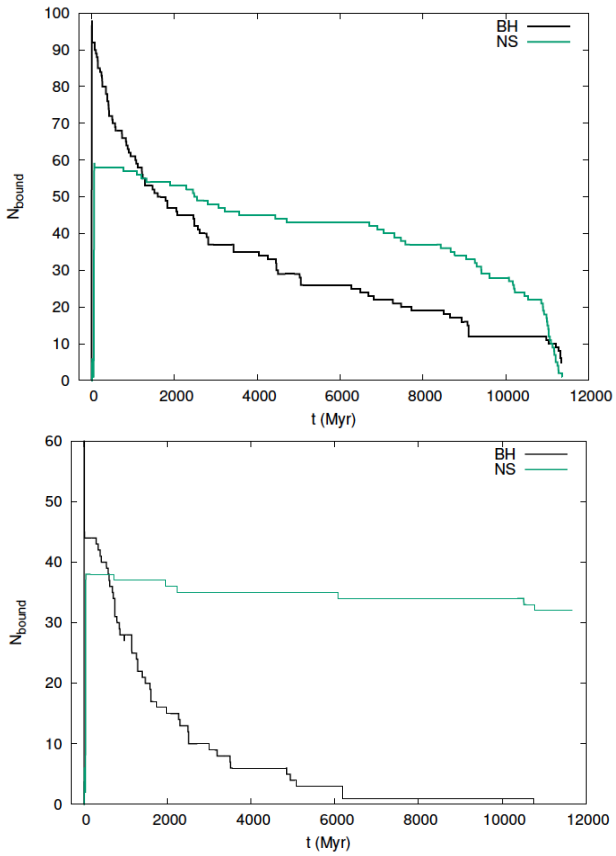

Figure 5: Examples of NBODY7 evolutions of the number of BHs and NSs bound to the cluster, for models with $M_{cl} = 3e4\text{M}_\odot$ and $r_{h(0)} = 2$ pc having metallicities $Z = 0.05Z_\odot$ (top) and $Z = Z_\odot$ (bottom) Banerjee 2017. We observe that higher Z leads to quicker dissipation of BH in clusters.

[1] A PYTHON implementation of these libraries is available from https://github.com/mgieles/clusterbh.

[2] A FORTRAN implementation of these libraries is available from https://github.com/antoninifabio/BHBdynamics.

4.2. clusterBHBdynamics

The complete description of the model can be found in Antonini and Gieles 2020, and only relevant aspects are discussed here.

clusterBHBdynamics makes use of Henon's principle (Hénon 1975), which states that the rate of heat generation in the core of a GC, $\dot{E}$, is a constant fraction of the total cluster energy per half-mass relaxation time, r_h, and that the flow of energy through the half-mass radius is independent of the precise mechanisms for energy production within the core. It is expressed mathematically as

$$\dot{E} = \gamma \frac{|E|}{t_{rh}} \tag{1}$$

where $E \approx -0.2GM_{cl}^2/r_h$ is the total energy of the cluster, γ is the a constant ≈ 0.1 and t_{r_h} average relaxation time scale within the r_h of the cluster (Alexander and Gieles 2012; M. Giersz and Heggie 1994). Structurally, the cluster is considered a two component system: a light component, consisting of stars, white dwarfs and neutron stars, and a heavy component of BHs.

Instead of evolving each body individually, Hénon 1961 used the fact that BHs in the core are the producers of heat in a balanced evolution, and thus their evolution can be linked to the properties of the host cluster. This enormously simplifies the computational load, since the model comes down to a series of coupled first order differential equations, which can be solved to derive various other parameters. These differential equations are for the rate of change of M_{cl}, r_h and the total M_{BH} with respect to time. The focus of this paper is BH binary formation and evolution, though these equations are of interest and can be found in section 2.3 of Antonini and Gieles 2020.

Initial conditions require $M_{cl(0)}$, $r_{h(0)}$ and the total $M_{BH(0)}$ at $t = 0$, the time of cluster formation. Since a cluster forms with all stars on the main sequence, $M_{BH} = 0$ initially, but for simplicity the evolution is begun at 20 Myr, to avoid simulating the first epoch, and instead make f_0 an input parameter of the model, where $f_0 = M_{BH(0)}/M_{cl(0)}$.

Analogously to the application of Henon's law in equation 1, the hardening of binaries in the core via binary-single interactions releases energy into the cluster, prompting the following relationship:

$$\dot{E}_{bin} = \dot{E} \tag{2}$$

where E_{bin} is the energy of the binary,

$$E_{bin} = Gm_1m_2/2a \tag{3}$$

a is the binary semimajor axis and m_1 and m_2 are the masses of the BH components. Since Henon's law states that the exact mechanism of energy propagation is irrelevant, equation 3 tells us the total energy released into the cluster by all BH mergers. Therefore, we can now consider the merging mechanisms simulated by clusterBHBdynamics:

4.2.1. *In-Cluster Inspirals*

As discussed in section 2, binaries experiencing binary-single interactions in the core exchange $\sim 20\%$ of energy and momentum with each encounter, contracting the semimajor axis until the binary evolution is dominated by GW energy loss (Antonini and Gieles 2020). The transition from dynamical to the GW emission regime of the binary occurs when eccentricity e within $l = (1 - e^2)^{1/2}$ passes the critical value

$$l < l_{GW} \approx 1.3 \left[\frac{G^3 (m_1 m_2)^2 m_{12}}{c^5 \dot{E}_{bin}} \right]^{1/7} a^{-5/7} \tag{4}$$

and thereafter the rate of change of the semi-major axis and eccentricity are governed by the following equations in clusterBHBdynamics (Peters 1964):

$$\dot{a}_{GW} = -\frac{64}{5} \frac{G^3 m_1 m_2 m_{12}}{c^5 a^3 l^7} \left(1 + \frac{73}{24} e^2 + \frac{37}{96} e^4\right) \tag{5}$$

$$\dot{e}_{GW} = -\frac{304}{15} \frac{G^3 m_1 m_2 m_{12}}{c^5 a^4 l^5} \left(e + \frac{121}{304} e^3\right) \tag{6}$$

where m_1 and m_2 the masses of the BH components, $m_{12} = m_1 + m_2$ and c is the speed of light in a vacuum.

Some interesting observations can be made using these equations. For clusters of a given velocity dispersion, and assuming equal mass BHs (i.e. $m_1 = m_2 = m$) we can write $a \propto m^2$. Using this, equation 5 yields $\dot{a}_{GW} \propto -m^{-3}$. The rate of contraction of the binary is therefore higher for lower mass BHs, which are found in GCs with high Z (Banerjee 2017).

Furthermore, if $a_{GW} \propto m^2$, then the inspiral timescale $t_{GW} = a_{GW}/\dot{a}_{GW} \propto m^5$, demonstrating the strong dependence on mass, with smaller BHs having shorter t_{GW}.

Therefore, we can infer that therefore higher Z leads to smaller timescales for inspiral mergers and that high-metallicity open clusters are favoured as sources of BBHs.

4.2.2. *GW Captures*

A merger may also form by direct gravitational capture during a three body encounter. Such events can only be probed with an N-body code that includes GR corrections and contribute $\leq$10% of all mergers in GCs (Banerjee 2018a). Relations derived from N-body simulations

by Samsing 2018 are used in clusterBHBdynamics, with the following GW capture (GWC) condition instated:

$$l < l_{GWC} \approx h \left(\frac{R_s}{a} \right)^{5/14} \tag{7}$$

where $R_s = 2Gm_{12}/c^2$, and h is a constant near unity. If this condition is met, a binary will merge before the next dynamic interaction occurs (Antonini and Gieles 2020). This population remains relatively unexplored, however may be of great significance applied to constraining the evolutionary stage of a GC, as its formation may leave characteristic signals in data obtained by LIGO and other laser interferometers (Samsing 2018).

4.2.3. Ejected Binaries

The last key mechanism of merging occurs in binaries ejected from their parent cluster. As previously discussed, this is the fate of most binaries due to v_{bin} eventually surpassing v_{esc} due to numerous binary-single interactions. The criterion applied in clusterBHBdynamics for an ejected binary is

$$l < l_{ej} \approx 1.8 \left(\frac{G^3 m_1 m_2 m_{12} \tau}{c^5} \right)^{1/7} a^{-4/7} \tag{8}$$

where τ is is the look-back time at which the binary was ejected. Since the simulated clusters are in equilibrium, the binary formation rate Γ_{bin} can be linked to the BH mass ejection rate, , via the relation

$$\Gamma_{bin} \approx - \frac{\dot{M}_{BH}}{m_{ej}} \tag{9}$$

where m_{ej} is the total mass ejected by each BH. This is one of the key equations in the model as it provides insight into the binary formation rate based only on global cluster properties, since the core's heating is affected only by the entire cluster's mass, radius and metallicity. One important result from eq. 9 is that at high Z, $\dot{M}_{BH}$ is smaller because each BH is smaller, and subsequently so is m_{ej}. Ultimately, the rate at which binaries form is higher at high Z.

With these relationships between cluster mass, radius, metallicity and time of evolution, clusterBHBdynamics is able to reproduce the binary formation rate, the rate of mergers and other variables, only by solving a set of first order differential equations. This gives the model great potential in extensively exploring the parameter space quickly, if the model agrees with today's N-body simulations within an acceptable uncertainty. Therefore the performance of the two models with the mechanisms discussed in this section considered, and systematic differences should be identified, if clusterBHBdynamics is to be used as a reliable exploratory tool. The methodology employed and the findings are discussed in the following sections.

4.3. Cluster Monte Carlo

The final model considered is the Cluster Monte Carlo (CMC) simulation from Rodriguez et al. 2018. It operates on similar principles to NBODY7, however is less taxing computationally and thus has been used to rigorously simulate regions of the parameter space unexplored by NBODY7. For example, masses tested by NBODY7 were capped at 1.0x10^5, while CMC offers GC simulations at various metallicities in the range 1.0x10^{5}M$_\odot$ $\leq M_{cl} \leq$ 4.0x10^{6}M$_\odot$, providing a more complete mass range for comparison with clusterBHBdynamics.

There are some key differences between the three models and their applications in current literature. Firstly, Banerjee 2020's application of NBODY7 is primarily to young massive and open stellar clusters, while Rodriguez et al. 2018's CMC and Antonini and Gieles 2020's clusterBHBdynamics focus on GCs. Their differences are discussed in section 1 and should be kept in mind when comparing the two models. Secondly, it is worth reiterating that the number of mergers from the direct N-body and MC models are discrete, while clusterBHBdynamics evolves key parameters through differential equations and therefore yields continuous output. This poses a comparative issue from a statistical point of view, and is addressed in the methodology section below.

5. METHODOLOGY

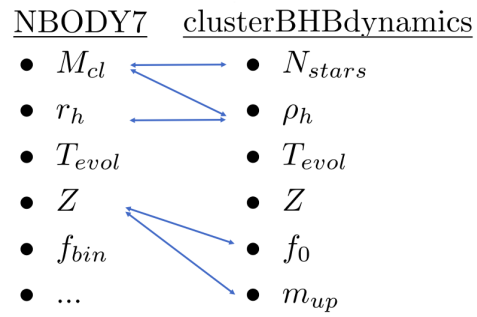

Figure 6: A table showing the key parameters of both models considered in this study, although both are able to consider additional input variables. Arrows indicate conversion pathways between related parameters.

Evolving only key parameters as opposed to a fully dynamic N-body simulation is immensely more computationally efficient, however, it is likelier to produce a less realistic output since key parameters may evolve differently, and since some second order variables are ignored. Therefore, there exists a motive to compare the

runs of the two models and quantify any excess mergers, to see if a mechanism not yet included in clusterBHBdynamics could be responsible for any systematic differences between the two models. As aforementioned, NBODY7 simulations were run on Graphics Processing Units (GPUs), with each run occupying hours to weeks of processing time. For this reason, all published runs from Banerjee 2017, Banerjee 2018a, Banerjee 2018b andBanerjee 2020 were compiled into a database of 110 merger simulations and used in this study. They can be seen in table II. These runs were then carried out in clusterBHBdynamics, after converting the initial conditions from NBODY7 runs to the closest possible initial conditions within clusterBHBdynamics.

This conversion of variables is non-trivial. Firstly, we note from the inputs of both models that clusterBHBdynamics requires the upper BH mass m_{up} and the initial BH fraction f_0 as inputs. This data is not available from NBODY7 runs and thus the standalone version of the SSE code of Hurley et al. 2000, with updates from Banerjee 2020 has been used to draw relationships between Z, f_0 and m_{up}. These relationships, shown in fig. 7, provide the conversion pathway for two arrowsindicated in table 5, starting from NBODY's Z. It is important to highlight that in the initial BH mass fraction, f_0, 'initial' does not refer to $t = 0$, since f_0 at $t = 0$ is zero. Instead, clusterBHBdynamics begins evolving at 20 Myr, to avoid simulating the first fractional epoch of the cluster.

Secondly, in addition to those listed in table 5, NBODY7 takes a further 3 input parameters: SN kicks, BH spin and various remnant models. The current version of clusterBHBdynamics does not facilitate these second order variables. This leads to the unavoidable issue of grouping NBODY7 parameters which clusterBHBdynamics cannot interpret, and comparing averages of these grouped runs with the corresponding clusterBHBdynamics simulations. Any systematic differences that may arise from this method are exactly the discrepancies this study aims to find, in order to prompt an adjustment relationship for clusterBHBdynamics.

If the fundamental mechanics behind both models agree, then plotting initial M_{cl} vs BH merger number N_{merg}, and thus grouping r_h and other variables together within mass bins, should in theory not show any systematic differences. Therefore, the numbers of mergers averaged over all variables (fig. 9) for given masses should show similar N_{merg}.

It can be of further interest to extract more specific groups of runs from the 110 simulations, with the goal of identifying which input parameters (or which ranges of given parameters) cause any systematic differences. We therefore proceed to split the 110 runs into hierarchical groups, according to the next most influential parameter after M_{cl}, which is r_h. Unfortunately, since the published NBODY7 and CMC runs are limited, this leaves only a handful of subsets with sufficient data points to make comparisons. The most abundant of these happens to be $r_h = 2$ pc, comprised of 74 runs and spanning 7 values of

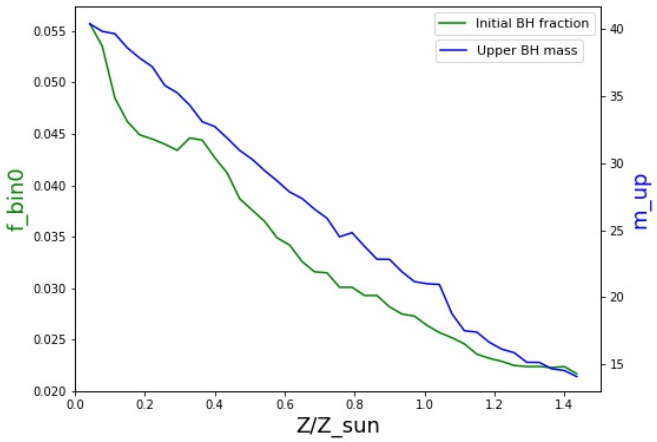

Figure 7: Initial cluster mass that ends up in BHs (f_0 in clusterBHBdynamics) and the maximum BH mass, m_{up}, as functions of metallicity, derived using a standalone version of the SSE code from Hurley et al. 2000, with updates from Banerjee 2020's NBODY7 code. These relations allow for comparison of f_0 and m_{up} in clusterBHBdynamics with Z in NBODY7.

M_{cl}. A plot of these runs as M_{cl} vs N_{merg} can be seen in fig. 10.

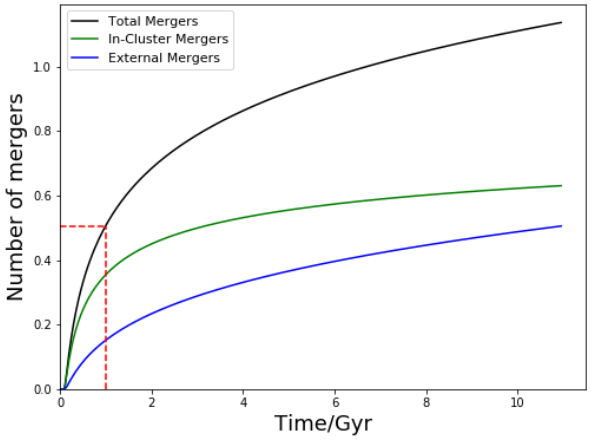

Figure 8: Run #108 from Table II showing typical output for the number of mergers as a function of time using clusterBHBdynamics. The near-plateau of the mergers within the cluster is a consequence of the dynamical extinction of BBH from the cluster core, or cluster 'dissolution'. In this particular run, the cluster 'dissolved' after 1 Gyr in NBODY7, and thus was cut off at this time clusterBHBdynamics, as indicated by the dashed red line.

The optimisation algorithm used to find the best fit was the downhill simplex, due to its sensitivity to errors in the data (Koshel 2002). The relationships that were fitted and optimised are

$$\psi_s = a_s \cdot M_{cl}^{b_s} \tag{10}$$

$$\psi_r = a_r \cdot M_{cl}^{b_r} + 1 \tag{11}$$

where ψ is the fit and a and b are constants determined by the algorithm[3]. In figures 9 and 10, ψ_s was used for plots with NBODY7 N_{merg} shown separately (top panels), while ψ_r was fitted to the ratios of N_{merg} for the two models (bottom panels). The additional constant of 1 for the ratio plots ensures that the fit levels off at larger cluster masses, since we know that clusterBHBdynamics is in good agreement with CMC for $M_{cl} > 1.0\text{x}10^6\text{M}_\odot$ from Antonini and Gieles 2020.

NBODY7 runs from Banerjee 2020's data are assumed to be Poisson-distributed, and hence each run has uncertainty $\delta N_i = \sqrt{N_i}$. Each run is then divided by the deterministic result of clusterBHBdynamics, M_i and averages are worked out for each mass bin as follows:

$$R_i \pm \delta R_i = \frac{N_i}{M_i} \pm \frac{\delta N_i}{M_i} \tag{12}$$

We then compute the average of R_i: $A_i = \langle R_i \rangle$, and the corresponding uncertainty, which with error propagation is

$$A_i \pm \delta A_i = \frac{1}{N_p}\sum_{i=1}^{N_p} R_i \pm \frac{1}{N_p}\sqrt{\sum_{i=1}^{N_p} \delta R_i^2} \tag{13}$$

Exact errors for the runs of masses $M_{cl} \geq 1.0\text{x}10^5\text{M}_\odot$ computed using CMC could not be obtained, though can be seen in fig. 6 of Antonini and Gieles 2020. The lowest mass cluster ($7\text{x}10^3\text{M}_\odot$, run #1 in table II) produced 0 mergers by NBODY7 simulations and was left out of the analysis, due to the differences in the continuity-discreteness nature of the NBODY7 with clusterBHBdynamics.

6. FINDINGS AND DISCUSSION

As mentioned in the previous section, it is desirable that N_{merg} averaged over all variables for given masses in fig. 10 and fig. 9 is the same for all models. As we see from the top panels of both figures, the data from NBODY7 and CMC connect the two ends of cluster masses with a fairly agreeable correlation, fitted by ψ_s to NBODY7 points only and extended to fit all masses. This reinforces each model's credibility as they were developed independently, and gives a wider cluster mass range for comparison with clusterBHBdynamics. While there is a clear discontinuity between clusterBHBdynamics and the N-body & MC simulations around $M_{cl} = 10.0\text{x}10^5\text{M}_\odot$, all models show convergence for higher M_{cl} and this can clearly be seen in the bottom panels.

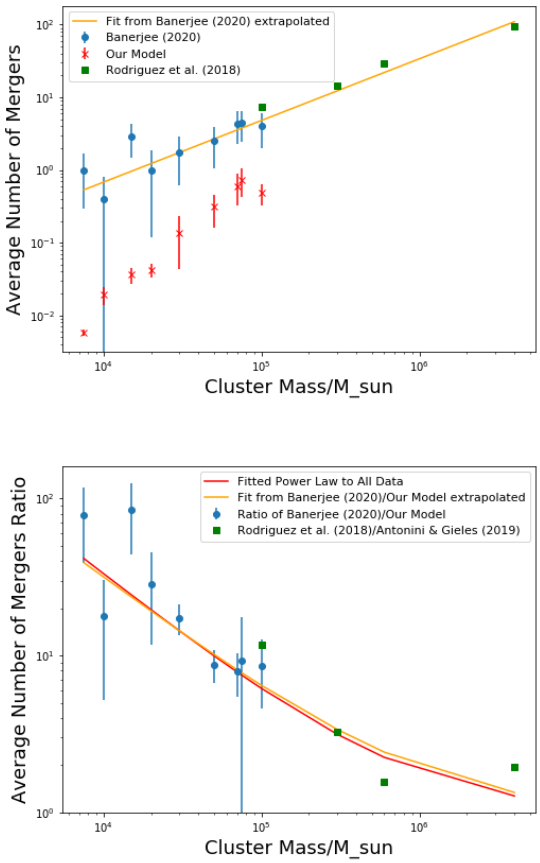

Figure 9: Top: N_{merg} vs M_{cl} for all runs from table II. The top plot shows the absolute number of plots from the 3 simulations with the downhill simplex fit for NBODY7, but data extrapolated for all masses. The yellow fit is NBODY/clusterBHBdynamics extrapolated for all data, while the red fit includes CMC/clusterBHBdynamics data. Bottom: R_i vs M_{cl} provides further insight into lower mass clusters, demonstrating that in fact, it is where the ratios diverge by most orders of magnitude.

The ratios of the number of mergers serve as more pedantic indicators of convergence, since both models produce very few mergers at lower M_{cl}. Here we see that the biggest disagreement, in fact, lies in the lower mass clusters, with clusterBHBdynamics predicting as many as 78.0 ± 39.1 times less mergers for $M_{cl} = 7.0\text{x}10^3\text{M}_\odot$, though the error is large, since only two runs are available at this mass.

We now examine the fits in the aforementioned plots using table I. Since a_{alldat} and a_{ext} for fig. 9 are more

[3] A PYTHON implementation of the adapted code is available from https://github.com/romanmikh/DownhillSimplexOptimization.

-	Fig. 9 Runs	Fig. 10	% Difference
a_{alldat}	48088.78	21901.90	-119.56
b_{alldat}	-0.79	-0.72	-9.72
a_{ext}	32049.22	108660.79	+339.04
b_{ext}	-0.75	-0.87	+13.79

Table I: Constants found for ψ_s and ψ_r using the downhill simplex optimisation fitter. a_{alldat} and a_{ext} refer to the multiplicative constant in equations 10 and 11 in fits for all data and extrapolated fits of only NBODY7/clusterBHBdynamics points, respectively. b_{alldat} and b_{ext} are the similarly defined exponents.

similar than a_{alldat} and a_{ext} for fig. 10, this tells us that all 110 datapoints averaged better agree with Rodriguez et al. 2018's data in the figures, which is also averaged for $r_h = 1$pc and 2pc. a_{alldat} and a_{ext} for only $r_h = 2$pc runs differ more, suggesting that clusterBHBdynamics output disagrees with CMC N_{merg} more at $r_h = 2$pc than at smaller radii. The change in sign of the constants in different figures amplifies this difference. Unfortunately, the sample size of $r_h = 1$ pc in table II is too small to repeat the same experiment and further data from NBODY7 and CMC would be required to conduct more rigorous studies of the dependence of N_{merg} to r_h in this manner.

Overall, however, b_{alldat} and b_{ext} (the dominant constants in equations 10 and 11) differ by 9.72% and 13.79% respectively in the two figures. Given the uncertainties involved in the ratio plots reach $\pm$ 50%, this is in reasonable agreement. This reinforces the findings in the lower panels of fig. 6 in Antonini and Gieles 2020, which showed convergence of clusterBHBdynamics with CMC at higher M_{cl}, however diverged at $M_{cl} <$ 1.0x10^{5}M$_\odot$. This ultimately suggests that clusterBHBdynamics is underestimating the number of mergers for $M_{cl} <$ 1.0x10^{5}M$_\odot$ when compared with NBODY7, and an adjustment to the code via a new physical mechanism is desirable.

The large difference in merger numbers for lower mass clusters in fig. 9 and 10 can in part be attributed to the continuity differences of the 3 models. N-body and Monte Carlo simulations either produce 0 or a discrete number of mergers, while clusterBHBdynamics yields a continuous function. Since the number of published runs from NBODY7 and CMC are limited, it has not been possible to conduct statistics with an ample sample size, which could bring the ratios in figs. 9 and 10 down slightly for low M_{cl}. This is one potential avenue to investigate in future studies.

Banerjee 2018b mentions the Kozai-Lidov (KL) oscillations in triple systems as a binary formation mechanism that deserves more attention, potent in lower mass clusters. KL oscillations occur when the inner orbit is inclined with respect to the outer orbit. The main feature of KL oscillations is the secular change of the eccentric-

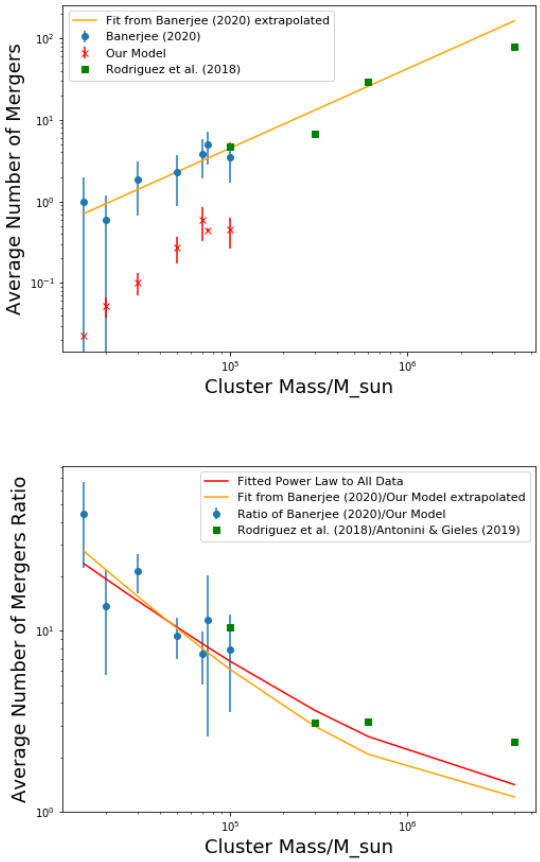

Figure 10: N_{merg} vs M_{cl} (top) and R_i vs M_{cl} (bottom) for all runs with $r_h = 2$pc from table II. The graphic structure is analogous to fig. 9

ity of the inner orbit and the relative inclination between the inner and outer orbits. More precisely, when the eccentricity decreases, the inclination increases, and vice versa. The eccentricity of the orbit can reach extreme values leading to various astrophysical phenomena. For instance, if the eccentricity becomes large enough, the merger rate of BHs can be enhanced by powerful GW emission (Kozai 1962; Lidov 1962; Gupta et al. 2020). In other words, although a star cluster ejects single and binary BHs and form BH-triples until its BH reservoir is (nearly) depleted (fig. 8, fig. 5), the occurrence of a dynamical BBH inspiral remains a probabilistic phenomenon. Additionally, in low ρ_h and M_{cl} clusters, the dynamically-formed triples can last unperturbed for a longer time, giving a higher chance to their inner binaries to merge via Kozai-Lidov oscillations Banerjee 2017. This mechanism could help resolve the discrepancy in N_{merg} currently seen at lower M_{cl}.

Goodman 1984 showed that the number of binaries in steady post-collapse evolution of a star cluster is higher in low-mass clusters. More specifically, the number of binaries N_{bin} depends on the number of stars in the clus-

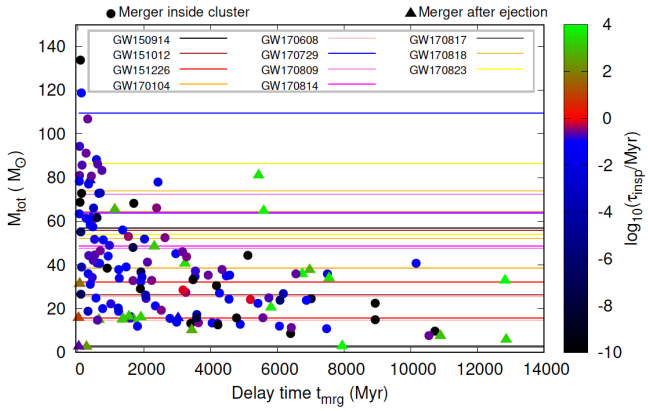

Figure 11: Total mass, M_{tot} vs merger delay time, t_{merg}, of GR compact-binary mergers from 65 of the 110 models computed in this study (Table C1, Banerjee 2020). Mergers are colour-coded according to their GR in-spiral times, τ_{insp} (colour bar). The circles represent mergers inside a model cluster while being bound to it and the triangles represent those happening in compact-binary systems after they get ejected from the cluster. The 90% credible intervals of the total masses and mass ratios of observed merger events are shown as horizontal lines.

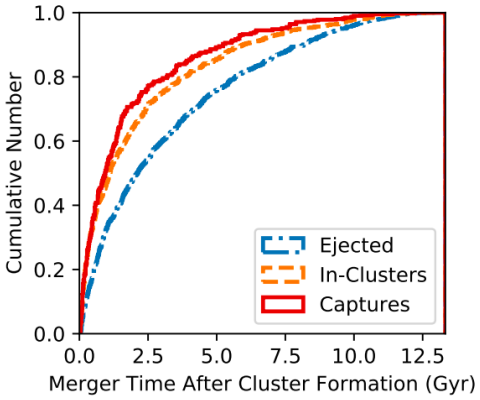

Figure 12: The cumulative distribution of t_{merg} for the ejected mergers, in-cluster mergers, and GW captures from Rodriguez et al. 2018's CMC model. As expected, the ejected BBHs typically merge later due to the large delay times between ejection and merging, that gravitational inspiral binaries experience. The in-cluster mergers and GW captures typically merge earlier, with nearly identical distributions.

ter N as $N_{bin} = N^{-1/3}$. At the same time, the number of stars in the core of the cluster N_{core} depends on N as $N_{core} = N^{1/3}$. This implies that the binary fraction in the core (i.e. $f_{bincore} = N_{bin}/N_{core)}$ depends on N as $f_{bin(core)} \sim N^{-2/3}$. Goodman 1984 also showed that for $N \approx 1.0\text{x}10^3$, the core binary fraction is about 25%. So, even without primordial binaries, low-mass clusters make more binaries and these cluster binary-binary interaction are more frequent. The binary-binary interactions are a viable route to producing stable hierarchical triple which could then produce a merger via the Lidov-Kozai mechanism (Gupta et al. 2020).

Binary-binary interactions can become significant in these conditions. We have seen that in steady-state, the dynamically formed binary fraction is higher lower M_{cl} (massive clusters tend to have 1 binary). Binary-binary interactions are therefore more common in low-mass clusters. Mikkola 1984 showed that binary-binary interactions lead to stable triples, which can also lead to the Lidov-Kozai mechanism and create in-cluster mergers.

Considering the discrepancy at low M_{cl} from another angle, we notice that in fig. 8, in-cluster and ejected binary mergers occur at a ratio close to one. This is typically seen in clusterBHBdynamics, while fig. 11 shows that in NBODY7, the majority of mergers are in-cluster and happen in very early evolution. The fact that Banerjee 2020 deals with young open clusters and Antonini and Gieles 2020 with GCs could be partly responsible for this difference, and thus it should be kept in mind that some systematic differences are expected.

6.1. Conclusion and Future Research

In conclusion, since small globular clusters are much more numerous, they are hosts to an abundance of black holes, and thus could be effective engines of binary BH mergers. Current models lead us to believe that the typical number of mergers produced by such a cluster is between 0 and 1 under typical conditions found in the Milky Way and similar galaxies, though with discrepancies from model to model. However, recent publications (Banerjee 2020; Rodriguez et al. 2018; Gupta et al. 2020) suggest previously unconsidered merger mechanisms that are of significance in small clusters specifically, and it is possible that current models are oversimplifying the evolutionary mechanics at low M_{cl}.

clusterBHBdynamics offers is a powerful tool for exploring stellar cluster and BH binary parameter space, due to its relative computational simplicity, though currently at the cost of accuracy for low mass clusters. The findings of this study suggest the implementation of Kozai-Lidov oscillations into the model could help bridge the discrepancy with NBODY7 in the number of mergers obtained. It would be worthwhile to study the implementation of more detaield SN kicks, BH spin and remnant models in clusterBHBdynamics during future studies.

The Laser Interferometer Space Antenna (LISA) is scheduled to launch in the 2030s for extraterrestrial GW observation, facilitating the observation of BH mergers at lower frequencies and shedding light on multi-band GW astrophysics (Antonini and Gieles 2020). Data from these observations will be invaluable for further development of cluster-BH coevolutionary models, and help clusterBHBdynamics realise its potential.

BIBLIOGRAPHY

Aarseth, Sverre J. (May 2012). "Mergers and ejections of black holes in globular clusters". In: 422.1, pp. 841–848. DOI: 10.1111/j.1365-2966.2012.20666.x. arXiv: 1202.4688 [astro-ph.SR].

Abbott, B. P. (2017a). "Observation of Gravitational Waves from a Binary Black Hole Merger". In: *Centennial of General Relativity: A Celebration*. Ed. by César Augusto Zen Vasconcellos, pp. 291–311. DOI: 10.1142/9789814699662_0011.

– (2017b). "Observation of Gravitational Waves from a Binary Black Hole Merger". In: *Centennial of General Relativity: A Celebration*. Ed. by César Augusto Zen Vasconcellos, pp. 291–311. DOI: 10.1142/9789814699662_0011.

Alexander, Poul E. R. and Mark Gieles (June 2012). "A prescription and fast code for the long-term evolution of star clusters". In: 422.4, pp. 3415–3432. DOI: 10.1111/j.1365-2966.2012.20867.x. arXiv: 1203.4744 [astro-ph.GA].

Antonini, Fabio, Enrico Barausse, and Joseph Silk (Oct. 2015). "The Coevolution of Nuclear Star Clusters, Massive Black Holes, and Their Host Galaxies". In: *Astrophys. J.* 812.1, 72, p. 72. DOI: 10.1088/0004-637X/812/1/72. arXiv: 1506.02050 [astro-ph.GA].

Antonini, Fabio and Mark Gieles (Feb. 2020). "Population synthesis of black hole binary mergers from star clusters". In: 492.2, pp. 2936–2954. DOI: 10.1093/mnras/stz3584. arXiv: 1906.11855 [astro-ph.HE].

Antonov, V. A. (1962). *Solution of the problem of stability of stellar system Emden's density law and the spherical distribution of velocities.*

Ashman, Keith M. and Stephen E. Zepf (Jan. 1992). "The Formation of Globular Clusters in Merging and Interacting Galaxies". In: *Astrophys. J.* 384, p. 50. DOI: 10.1086/170850.

Banerjee, Sambaran (May 2017). "Stellar-mass black holes in young massive and open stellar clusters and their role in gravitational-wave generation". In: 467.1, pp. 524–539. DOI: 10.1093/mnras/stw3392. arXiv: 1611.09357 [astro-ph.HE].

– (Jan. 2018a). "Stellar-mass black holes in young massive and open stellar clusters and their role in gravitational-wave generation - II". In: 473.1, pp. 909–926. DOI: 10.1093/mnras/stx2347. arXiv: 1707.00922 [astro-ph.HE].

– (Dec. 2018b). "Stellar-mass black holes in young massive and open stellar clusters and their role in gravitational-wave generation III: dissecting black hole dynamics". In: 481.4, pp. 5123–5145. DOI: 10.1093/mnras/sty2608. arXiv: 1805.06466 [astro-ph.HE].

– (Apr. 2020). "Stellar-mass black holes in young massive and open stellar clusters and their role in gravitational-wave generation IV: updated stellar-evolutionary and black hole spin models and comparisons with the LIGO-Virgo O1/O2 merger-event data". In: *arXiv e-prints*, arXiv:2004.07382, arXiv:2004.07382. arXiv: 2004.07382 [astro-ph.HE].

Banerjee, Sambaran and Pavel Kroupa (Jan. 2017). "How can young massive clusters reach their present-day sizes?" In: 597, A28, A28. DOI: 10.1051/0004-6361/201526928. arXiv: 1510.04293 [astro-ph.GA].

Fragione, Giacomo and Bence Kocsis (Oct. 2018). "Black Hole Mergers from an Evolving Population of Globular Clusters". In: *Phys. Rev. Lett.* 121.16, 161103, p. 161103. DOI: 10.1103/PhysRevLett.121.161103. arXiv: 1806.02351 [astro-ph.GA].

Gieles, Mark and Alice Zocchi (Nov. 2015). "A family of lowered isothermal models". In: 454.1, pp. 576–592. DOI: 10.1093/mnras/stv1848. arXiv: 1508.02120 [astro-ph.IM].

Giersz, M. and D. C. Heggie (Sept. 1994). "Statistics of N-Body Simulations - Part Two - Equal Masses after Core Collapse". In: 270, p. 298. DOI: 10.1093/mnras/270.2.298. arXiv: astro-ph/9403024 [astro-ph].

Giersz, Mirek et al. (May 2013). "MOCCA code for star cluster simulations - II. Comparison with N-body simulations". In: 431.3, pp. 2184–2199. DOI: 10.1093/mnras/stt307. arXiv: 1112.6246 [astro-ph.GA].

Goodman, J. (May 1984). "Homologous evolution of stellar systems after core collapse". In: *Astrophys. J.* 280, pp. 298–312. DOI: 10.1086/161996.

Gupta, Priti et al. (May 2020). "Gravitational waves from hierarchical triple systems with Kozai-Lidov oscillation". In: *Phys. Rev. D* 101.10, 104053, p. 104053. DOI: 10.1103/PhysRevD.101.104053. arXiv: 1911.11318 [gr-qc].

Hénon, M. (Feb. 1961). "Sur l'évolution dynamique des amas globulaires". In: *Annales d'Astrophysique* 24, p. 369.

– (Jan. 1975). "Two Recent Developments Concerning the Monte Carlo Method". In: *Dynamics of the Solar Systems*. Ed. by Avram Hayli. Vol. 69. IAU Symposium, p. 133.

Hurley, J. R. et al. (Jan. 2000). "On the Road to Realistic Globular Cluster Models". In: *Astronomische Gesellschaft Meeting Abstracts*. Ed. by Reinhard E. Schielicke. Astronomische Gesellschaft Meeting Abstracts.

Jordán, Andrés et al. (July 2007). "The ACS Virgo Cluster Survey. XII. The Luminosity Function of Globular Clusters in Early-Type Galaxies". In: 171.1, pp. 101–145. DOI: 10.1086/516840. arXiv: astro-ph/0702496 [astro-ph].

Koshel, R. John (Dec. 2002). "Enhancement of the downhill simplex method of optimization". In: vol. 4832. Society of Photo-Optical Instrumentation Engineers (SPIE) Conference Series, pp. 270–282. DOI: 10.1117/12.486465.

Kozai, Yoshihide (June 1962). "Secular Perturbations of Asteroids with High Inclination and Eccentricity." In: 67, p. 579. DOI: 10.1086/108876.

Kumamoto, Jun, Michiko S. Fujii, and Ataru Tanikawa (May 2020). "Merger rate density of binary black holes formed in open clusters". In: 495.4, pp. 4268–4278. DOI: 10.1093/mnras/staa1440. arXiv: 2001.10690 [astro-ph.HE].

Kuroda, K. and LCGT Collaboration (Apr. 2010). "Status of LCGT". In: *Classical and Quantum Gravity* 27.8, 084004, p. 084004. DOI: 10.1088/0264-9381/27/8/084004.

Lane, Richard R. et al. (Mar. 2010). "AAOmega Observations of 47 Tucanae: Evidence for a Past Merger?" In: 711.2, pp. L122–L126. DOI: 10.1088/2041-8205/711/2/L122. arXiv: 1002.0625 [astro-ph.GA].

Leonard, Peter J. T. (July 1989). "Stellar Collisions in Globular Clusters and the Blue Straggler Problem". In: 98, p. 217. DOI: 10.1086/115138.

Lidov, M. L. (Oct. 1962). "The evolution of orbits of artificial satellites of planets under the action of gravitational perturbations of external bodies". In: 9.10, pp. 719–759. DOI: 10.1016/0032-0633(62)90129-0.

Liu, Chang et al. (June 2020). "Multiband observation of LIGO/Virgo binary black hole mergers in the gravitational-wave transient catalog GWTC-1". In: 496.1, pp. 182–196. DOI: 10.1093/mnras/staa1512. arXiv: 2004.12096 [astro-ph.HE].

Mann, Adam (Mar. 2020). "The golden age of neutron-star physics has arrived". In: *Nature (London)* 579.7797, pp. 20–22. DOI: 10.1038/d41586-020-00590-8.

Merafina, Marco, Kristian Piscicchia, and Martina Donnari (Jan. 2018). "Gravity and thermodynamics in globular clusters: Theoretical developments and results by numerical simulations". In: *Fourteenth Marcel Grossmann Meeting - MG14*. Ed. by Massimo Bianchi, Robert T. Jansen, and Remo Ruffini, pp. 2509–2514. DOI: 10.1142/9789813226609_0298.

Mikkola, S. (Mar. 1984). "Encounters of binaries. II - Unequal energies". In: 207, pp. 115–126. DOI: 10.1093/mnras/207.1.115.

Nitadori, Keigo and Sverre J. Aarseth (July 2012). "Accelerating NBODY6 with graphics processing units". In: 424.1, pp. 545–552. DOI: 10.1111/j.1365-2966.2012.21227.x. arXiv: 1205.1222 [astro-ph.IM].

Peters, Philip Carl (Jan. 1964). "Gravitational radiation and the motion of two point masses". PhD thesis. California Institute of Technology.

Plummer, H. C. (Mar. 1911). "On the problem of distribution in globular star clusters". In: 71, pp. 460–470. DOI: 10.1093/mnras/71.5.460.

Portegies Zwart, Simon F., Stephen L. W. McMillan, and Mark Gieles (Sept. 2010). "Young Massive Star Clusters". In: 48, pp. 431–493. DOI: 10.1146/annurev-astro-081309-130834. arXiv: 1002.1961 [astro-ph.GA].

Rodriguez, Carl L. et al. (Dec. 2018). "Post-Newtonian dynamics in dense star clusters: Formation, masses, and merger rates of highly-eccentric black hole binaries". In: *Phys. Rev. D* 98.12, 123005, p. 123005. DOI: 10.1103/PhysRevD.98.123005. arXiv: 1811.04926 [astro-ph.HE].

Samsing, Johan (May 2018). "Eccentric black hole mergers forming in globular clusters". In: *Phys. Rev. D* 97.10, 103014, p. 103014. DOI: 10.1103/PhysRevD.97.103014. arXiv: 1711.07452 [astro-ph.HE].

Spitzer Lyman, Jr. and Richard Harm (May 1958). "Evaporation of Stars from Isolated Clusters." In: *Astrophys. J.* 127, p. 544. DOI: 10.1086/146486.

Table II: A complete summary of the 100 model evolutionary calculations performed in this study. The columns from left to right give the model cluster's (a) ID number, (b) initial mass, M_{cl}, (c) initial half-mass radius, r_h, (d) metallicity in solar units, $Z/Z_{\odot}$, (e) initial fraction of primordial binaries, f_{bin0}, (f) model evolutionary time, T_{evol}, (g) number of BH mergers produced by NBODY7, N_{mergN}, (h) number stars within the cluster, assuming a uniform solar mass of 0.638M$_{\odot}$, N_{stars}, (i) half radius cluster density, ρ_h, (j) initial (20 Myr is treated as $t = 0$ in clusterBHBdynamics) BH fraction of the cluster, f_0, (k) upper BH mass, m_{up}, and (l) is the number of BH mergers produced by clusterBHBdynamics, N_{mergC}. Columns (a), (c) and (e) are specific to NBODY7 and were converted to clusterBHBdynamics variables (h), (i), (j) and (k) by relations discussed in section 5. Columns (b), (d), (f), (g) and (k) are either mutual parameters for both models or are the outputs of the models.

Run#	M_{cl}	r_h	$Z/Z_{\odot}$	f_{bin0}	T_{evol}	N_{mergN}	N_{stars}	ρ_h	f_0	m_{up}	N_{mergC}
1	7000	1	0.05	0	7	0	10971.7	835.56	0.055	40	0.0116
2	7500	1	0.05	0.5	5.2	2	11755.4	895.24	0.055	40	0.0128
3	7500	1	1	0.5	2.4	0	11755.4	895.24	0.026	21	0.016
4	10000	2	0.05	0	9	0	15673.9	149.20	0.055	40	0.0107
5	10000	1	0.05	0	5	1	15673.9	1193.6	0.055	40	0.022
6	10000	1	0.07	0.1	8.5	0	15673.9	1193.6	0.054	38	0.025
7	10000	1	0.07	0.1	5.2	1	15673.9	1193.6	0.054	38	0.023
8	10000	1	0.25	0	5	0	15673.9	1193.6	0.044	36	0.023
9	15000	2	0.05	0	10	1	23510.9	223.81	0.055	40	0.0225
10	15000	1.5	0.05	0.05	6.6	2	23510.9	530.51	0.055	40	0.03
11	15000	1.5	0.05	0.05	9.4	14	23510.9	530.51	0.055	40	0.032
12	15000	1.5	0.05	0.3	11	3	23510.9	530.51	0.055	40	0.034
13	15000	1.5	0.05	0.5	4.9	1	23510.9	530.51	0.055	40	0.028
14	15000	1	0.25	0	5	0	23510.9	1790.4	0.044	36	0.05
15	15000	1.5	0.25	0.05	9.9	5	23510.9	530.51	0.044	36	0.0355
16	15000	1.5	1	0.05	11	3	23510.9	530.51	0.026	21	0.05
17	15000	1.5	1	0.3	2.2	3	23510.9	530.51	0.026	21	0.042
18	15000	1.5	1	0.5	2.1	2	23510.9	530.51	0.026	21	0.041
19	15000	1.5	1	0.3	4.6	1	23510.9	530.51	0.026	21	0.045
20	15000	1.5	1	0.5	0.75	2	23510.9	530.51	0.026	21	0.027
21	20000	2	0.07	0.1	11	1	31347.9	298.41	0.054	38	0.0415
22	20000	2	0.07	0.1	8.7	1	31347.9	298.41	0.054	38	0.039
23	20000	2	0.71	0.1	4.4	0	31347.9	298.41	0.032	26	0.05
24	20000	2	0.71	0.1	5.8	1	31347.9	298.41	0.032	26	0.0535
25	20000	2	1.42	0.1	4.4	0	31347.9	298.41	0.022	14	0.08
26	30000	1	0.01	0	11	3	47021.9	3580.9	0.059	43	0.183
27	30000	2	0.01	0	11	1	47021.9	447.62	0.059	43	0.075
28	30000	3	0.01	0	6.6	0	47021.9	132.62	0.059	43	0.039
29	30000	2	0.05	0	10	3	47021.9	447.62	0.055	40	0.08
30	30000	2	0.05	0.02	10	1	47021.9	447.62	0.055	40	0.08
31	30000	2	0.05	0.05	10	1	47021.9	447.62	0.055	40	0.08
32	30000	2	0.05	0.1	10	3	47021.9	447.62	0.055	40	0.08
33	30000	2	0.05	0.05	10.2	1	47021.9	447.62	0.055	40	0.08
34	30000	2	0.05	0.1	10.2	3	47021.9	447.62	0.055	40	0.08
35	30000	2	0.07	0.1	11	2	47021.9	447.62	0.054	38	0.086
36	30000	2	0.07	0.1	11	0	47021.9	447.62	0.054	38	0.086
37	30000	2	0.07	0.1	11	3	47021.9	447.62	0.054	38	0.086
38	30000	2	0.07	0.1	9.3	1	47021.9	447.62	0.054	38	0.082
39	30000	2	0.25	0	10	2	47021.9	447.62	0.044	36	0.089
40	30000	2	0.25	0.02	10	2	47021.9	447.62	0.044	36	0.089
41	30000	2	0.25	0.05	10	4	47021.9	447.62	0.044	36	0.089
42	30000	2	0.25	0.1	6	3	47021.9	447.62	0.044	36	0.079
43	30000	2	0.25	0.05	10.1	4	47021.9	447.62	0.044	36	0.089
44	30000	2	0.25	0.05	10.9	5	47021.9	447.62	0.044	36	0.09
45	30000	2	0.25	0.1	6.3	3	47021.9	447.62	0.044	36	0.08

$Run\#$	M_{cl}	r_h	$Z/Z_\odot$	f_{bin0}	T_{evol}	N_{mergN}	N_{stars}	ρ_h	f_0	m_{up}	N_{mergC}
46	30000	1	0.71	0	7.2	2	47021.9	3580.9	0.032	26	0.25
47	30000	1	0.71	0	11	2	47021.9	3580.9	0.032	26	0.27
48	30000	1	0.71	0	10.9	4	47021.9	3580.9	0.032	26	0.27
49	30000	2	0.71	0	9.7	2	47021.9	447.62	0.032	26	0.124
50	30000	2	0.71	0	11	2	47021.9	447.62	0.032	26	0.127
51	30000	2	0.71	0.1	11	0	47021.9	447.62	0.032	26	0.127
52	30000	2	0.71	0.1	11	1	47021.9	447.62	0.032	26	0.127
53	30000	3	0.71	0	11	3	47021.9	132.62	0.032	26	0.074
54	30000	3	0.71	0	11	0	47021.9	132.62	0.032	26	0.074
55	30000	2	1	0	10	1	47021.9	447.62	0.026	21	0.14
56	30000	2	1	0.05	10.9	1	47021.9	447.62	0.026	21	0.142
57	30000	1	1.42	0	11	0	47021.9	3580.9	0.022	14	0.41
58	30000	1	1.42	0	8.2	0	47021.9	3580.9	0.022	14	0.4
59	30000	1	1.42	0	7	1	47021.9	3580.9	0.022	14	0.39
60	30000	2	1.42	0	11	0	47021.9	447.62	0.022	14	0.2
61	30000	2	1.42	0.1	3	0	47021.9	447.62	0.022	14	0.15
62	30000	3	1.42	0	10.1	2	47021.9	132.62	0.022	14	0.127
63	30000	3	1.42	0	11	0	47021.9	132.62	0.022	14	0.13
64	50000	2	0.00	0.05	11	2	78369.9	746.03	0.059	43	0.19
65	50000	2	0.00	0.05	11	4	78369.9	746.03	0.059	43	0.19
66	50000	2	0.01	0	11	1	78369.9	746.03	0.059	43	0.19
67	50000	2	0.01	0	11	1	78369.9	746.03	0.059	43	0.19
68	50000	2	0.05	0	10	2	78369.9	746.03	0.055	40	0.19
69	50000	2	0.05	0.05	11	3	78369.9	746.03	0.055	40	0.2
70	50000	2	0.07	0	11	2	78369.9	746.03	0.054	38	0.22
71	50000	2	0.07	0	11	0	78369.9	746.03	0.054	38	0.22
72	50000	2	0.07	0	11	2	78369.9	746.03	0.054	38	0.22
73	50000	2	0.07	0.05	10	6	78369.9	746.03	0.054	38	0.21
74	50000	2	0.07	0.05	11	3	78369.9	746.03	0.054	38	0.22
75	50000	1	0.07	0	11	3	78369.9	5968.3	0.054	38	0.55
76	50000	1	0.07	0	11	3	78369.9	5968.3	0.054	38	0.55
77	50000	1	0.07	0	11	5	78369.9	5968.3	0.054	38	0.55
78	50000	2	0.25	0	10	1	78369.9	746.03	0.044	36	0.22
79	50000	2	0.25	0.05	11	4	78369.9	746.03	0.044	36	0.23
80	50000	2	0.35	0	11	1	78369.9	746.03	0.044	34	0.245
81	50000	2	0.35	0	11	4	78369.9	746.03	0.044	34	0.245
82	50000	2	0.71	0	11	1	78369.9	746.03	0.032	26	0.33
83	50000	2	0.71	0	11	3	78369.9	746.03	0.032	26	0.33
84	50000	2	0.71	0.05	11	2	78369.9	746.03	0.032	26	0.33
85	50000	1	0.71	0	11	7	78369.9	5968.3	0.032	26	0.72
86	50000	2	1	0	10	3	78369.9	746.03	0.026	21	0.375
87	50000	2	1	0.05	11	2	78369.9	746.03	0.026	21	0.39
88	50000	2	1	0.05	2.8	2	78369.9	746.03	0.026	21	0.235
89	50000	2	1.42	0	9.9	0	78369.9	746.03	0.022	14	0.52
90	50000	2	1.42	0	11	3	78369.9	746.03	0.022	14	0.53
91	50000	1	1.42	0	11	8	78369.9	5968.3	0.022	14	1.13
92	70000	2	0.00	0.05	11	3	109717.	1044.4	0.059	43	0.355
93	70000	2	0.07	0	11	2	109717.	1044.4	0.054	38	0.405
94	70000	2	0.07	0	11	3	109717.	1044.4	0.054	38	0.405
95	70000	2	0.07	0	11	3	109717.	1044.4	0.054	38	0.405
96	70000	2	0.07	0.05	11	5	109717.	1044.4	0.054	38	0.405
97	70000	2	0.07	0.05	9.8	6	109717.	1044.4	0.054	38	0.39
98	70000	2	0.35	0	11	4	109717.	1044.4	0.044	34	0.45
99	70000	2	0.71	0	11	6	109717.	1044.4	0.032	26	0.6
100	70000	2	0.71	0.05	11	2	109717.	1044.4	0.032	26	0.6
101	70000	2	1.42	0	11	6	109717.	1044.4	0.022	14	1.04
102	70000	2	1.42	0	11	4	109717.	1044.4	0.022	14	1.04
103	70000	2	1.42	0.05	11	2	109717.	1044.4	0.022	14	1.04
104	75000	2	0.05	0	10	7	117554.	1119.0	0.055	40	0.425
105	75000	2	0.25	0	10	3	117554.	1119.0	0.044	36	0.465

$Run\#$	M_{cl}	r_h	$Z/Z_\odot$	f_{bin0}	T_{evol}	N_{mergN}	N_{stars}	ρ_h	f_0	m_{up}	N_{mergC}
106	100000	2	0.05	0	1	3	156739.	1492.0	0.055	40	0.4
107	100000	2	0.07	0	11	6	156739.	1492.0	0.054	38	0.77
108	100000	1.5	0.07	0.05	1	4	156739.	3536.7	0.054	38	0.5
109	100000	2	0.25	0	1	4	156739.	1492.0	0.044	36	0.3
110	100000	2	0.5	0	1	1	156739.	1492.0	0.038	30	0.34